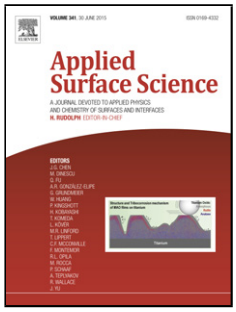

Title: Surface nanostructuring of thin film composite membranes via grafting polymerization and incorporation of ZnO nanoparticles

Author: Heba Isawi Magdi H. El-Sayed Xianshe Feng Hosam Shawky Mohamed S. Abdel-Mottaleb

PII: S0169-4332(16)31171-0
DOI: http://dx.doi.org/doi:10.1016/j.apsusc.2016.05.141
Reference: APSUSC 33334

To appear in: *APSUSC*

Received date: 25-2-2016
Revised date: 24-5-2016
Accepted date: 26-5-2016

Please cite this article as: Heba Isawi, Magdi H.El-Sayed, Xianshe Feng, Hosam Shawky, Mohamed S.Abdel-Mottaleb, Surface nanostructuring of thin film composite membranes via grafting polymerization and incorporation of ZnO nanoparticles, Applied Surface Science http://dx.doi.org/10.1016/j.apsusc.2016.05.141

Surface nanostructuring of thin film composite membranes via grafting polymerization and incorporation of ZnO nanoparticles

Heba Isawi[a,b*], Magdi H. El-Sayed[a], Xianshe Feng [b],

Hosam Shawky[a], Mohamed S. Abdel-Mottaleb[c]

[a] Desert Research Center, Hydrogeochemistry Dept., Cairo, Egypt

hebaessawi@hotmail.com[*]

[b] Department of Chemical Engineering, University of Waterloo, Waterloo, Ontario, Canada

[c]Faculty of Science, Ain Shams University, Cairo, Egypt

Highlights

1- Synthesis and characterization of ZnO nanoparticles

2- Use ZnO nanoparticles for membrane surface modifications

3- Characterization of TFC modified membrane

4- Effect of ZnO nanoparticles on membrane biofouling, hydrophilicity and salt rejection

Abstract

A new approach for modification of polyamid thin film composite membrane PA(TFC) using synthesized ZnO nanoparticles (ZnO NPs) was shown to enhance the membrane performances for reverse osmosis water desalination. First, active layer of synthesis PA(TFC) membrane was activated with an aqueous solution of free radical graft polymerization of hydrophilic methacrylic acid (MAA) monomer onto the surface of the PA(TFC) membrane resulting PMAA-g-PA(TFC). Second, the the PA(TFC) membrane has been developed by incorporation of ZnO NPs into the MAA grafting solution resulting the ZnO NPs modified PMAA-g-PA(TFC) membrane. The surface properties of the synthesized nanoparticles and prepared membranes were investigated using the FTIR, XRD and SEM. Morphology studies demonstrated that ZnO NPs have been successfully incorporated into the active grafting layer over PA(TFC) composite membranes. The zinc leaching from the ZnO NPs modified PMAA-g-PA(TFC) was minimal, as shown by batch tests that indicated stabilization of the ZnO NPs on the membrane surfaces. Compared with the a pure PA(TFC) and PMAA-g-PA(TFC) membranes, the ZnO NPs modified PMAA-g-PA(TFC) was more hydrophilic, with an improved water contact angle (~50 ± 3°) over the PMAA-g-PA(TFC) (63 ± 2.5°). The ZnO NPs modified PMAA-g-PA(TFC) membrane showed salt rejection of 97% (of the total groundwater salinity), 99% of dissolved bivalent ions (Ca^{2+}, $SO_4^{2-}$and Mg^{2+}), and 98% of mono valent ions constituents (Cl^- and Na^+). In addition, antifouling performance of the membranes was determined using *E. coli* as a potential foulant. This demonstrates that the ZnO NPs modified PMAA-g-PA(TFC) membrane can significantly improve the membrane performances and was favorable to enhance the selectivity, permeability, water flux, mechanical properties and the bio-antifouling properties of the membranes for water desalination.

Keywords:

ZnO Nanoparticles, Desalination, Grafting, Antifouling, Morphology, Reverse osmosis

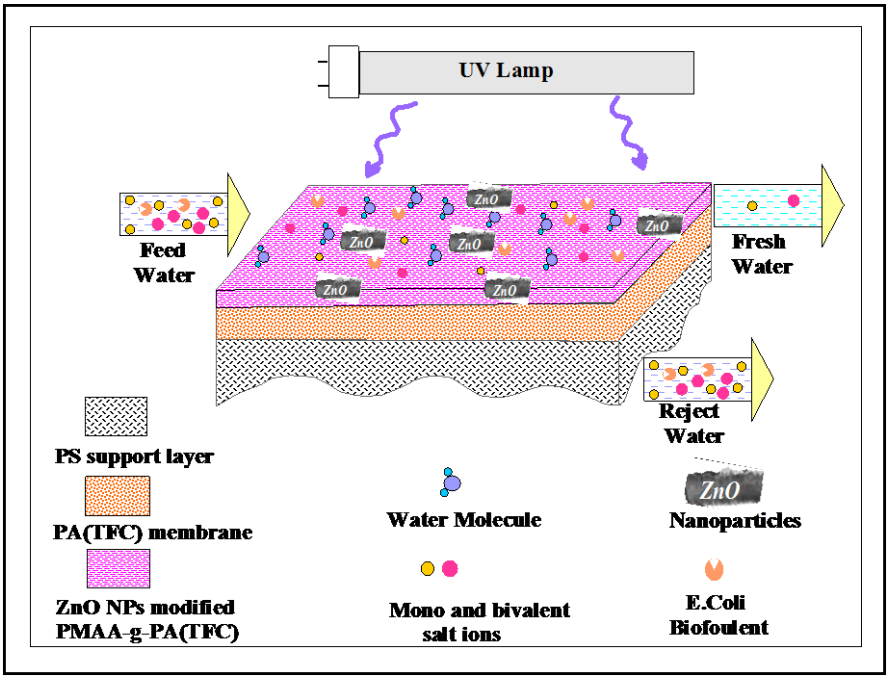

Graphical abstract

1. Introduction

Membrane separation is one of the most important tools for water desalination, as it offers high efficiency, stability, easy operation, and low energy requirements [1]. Likewise, reverse osmosis is considered the most promising technology utilized for water desalination [2]. The development of nanotechnology has resulted in enhanced membrane performance via the addition of new functional groups through surface modifications, and improvements to the membrane chemical structure [3]. Recent studies have demonstrated grafting and nano-surface membrane modifications lead to improved membrane performance, with improvements to: selectivity, bioantifouling properties, chemical stability, hydrophilicity, water flux, salt rejection, and mechanical properties [4].

Recently, thin film composite (TFC) membranes are the most commonly used membranes for reverse osmosis applications [5]. In typical TFC membranes, the thin skin barrier layer is created by interfacial polymerization of polyamide (PA) between two reactive monomers resulting in a PA(TFC) on top of a microporous supportive layer [6]. The most applicable supportive layer used in reverse osmosis is made of polysulfone (PS) due to its high mechanical, chemical and thermal stability, which is related to the operating pressure applied through the membrane. The PA(TFC) membrane surface characteristics could be modified by combining with a hydrophilic modifier through graft polymerization using a water-soluble polymer or using inorganic nanoparticles [7-9].

Graft polymerization is a common modification method used to improve the surface characteristics of the PA(TFC) membranes [10]. The methacrylic acid (MAA) monomer was selected for grafting polymerization in an aqueous solution by redox initiated radical grafting, resulting in a PMAA-g-PA(TFC) membrane. The MAA is compatible with the PA membrane, has high water solubility [11], and excellent biocompatibility [12]. Furthermore, the MAA monomers have been previously used in graft polymerization of RO membranes, and have shown a reasonable fouling reduction with no loss in water permeability. We demonstrate here that the incorporation of zinc oxide nanoparticles (ZnO NPs), with an aqueous grafting solution of MAA, can be used to modify the surface of a PA(TFC) membrane creating a ZnO modified PMAA-g-PA(TFC) membrane. The ZnO NPs modified PMAA-g-PA(TFC) membrane has been characterized, and its performances has been tested and compared with pure PA(TFC) and PMAA-g-PA(TFC) membranes. This comparison illustrates the impact of nanoparticle incorporation for enhancing membrane performance, and improving antifouling properties and mechanical characteristics. The ZnO NPs possess an –OH group on their surface, which links with the carboxylic group in the MAA grafting monomer by a covalent or hydrogen bond [13,14] facilitating this incorporation, and increasing the stability of the ZnO NPs on the membrane surface.

Recent advances in nanotechnology are greatly exploring ideas related to structures modifications and morphologies of the PA(TFC) membranes, allowing improved membrane performance and antifouling properties. Furthermore, many types of nanoparticles have been studied to enhance the membrane properties focus on SiO_2 [15], carbon nanotubes [16], silver nanoparticles [17], zeolites [18], Al_2O_3 [19], ZrO_2 [20], graphene oxide nanoparticles [21] and TiO_2 nanoparticles [22], which are relatively expensive for practical application. Zinc oxide nanoparticles have also been used as additives for membrane modifications as they possess unique physical and chemical properties, including; high chemical, thermal, mechanical and photo-stability, and an ideal electrochemical coupling coefficient. ZnO NPs possess a crystallographic structure at the

nano level [23], and can easily absorb hydroxyl groups (–OH) to become hydrophilic, which enhances membrane performance [24]. ZnO NPs are also a multifunctional material [25], with high ultraviolet resistance and photocatalytic properties [26]. Furthermore, membrane fouling is one of the most persistent problems impeding the practical application of membrane technology because it causes a decrease in salt rejection, water flux, and increases in the operational cost of the system [27]. Fouling is caused by the adsorption of organic compounds onto the membrane surface with many kinds of fouling possible, including; crystalline, organic, particulate, and microbial [28]. Due to the antibacterial and antifungal characteristics of the ZnO NPs, they have been widely used for the disinfection and decomposition of organic compounds [29], and consequently improve membrane bio-fouling resistance.

In this work ZnO NPs incorporated with MAA grafting solution were successfully synthesized using the hydrothermal technique, and then used as an additive to enhance the surface modification and application of PA(TFC) membranes. The stability of the ZnO NPs incorporated into the surface of the ZnO NPs modified PMAA-g-PA(TFC) membrane was investigated to assess the possible environmental risks of releasing ZnO NPs at high load. Therefore, a batch test was carried out to chemically restrain ZnO NPs on the membrane surface, and determine the release of the Zn^{2+} ion into the contact solution of distilled water over long time periods. The chemical composition and morphology of the ZnO NPs and the modified membrane were characterized through: X-ray spectroscopy (X-ray), Fourier transform infrared spectroscopy (FTIR), Scanning electron microscope (SEM), transmission electron microscopy (TEM), thermogravimetric analysis (TGA), assessments of mechanical property, contact angle (CA) determination, and tests of ZnO NP stability on the membrane surface. Through these experiments, the optimum amount of ZnO NPs was proposed, and the reaction mechanism of preparation, separation of the natural groundwater, and bio-antifouling effect caused by additive ZnO NPs was also examined.

The novelty of this research is the incorporation of the synthesized ZnO NPs with the grafting MAA aqueous solution and the subsequent improvements to the performance of reverse osmosis technology in terms of water flux, salt rejection, and bio-antifouling using *E. coli* as a model organism and potential foulant. Furthermore, the stability of the ZnO NPs on the membrane surface over time will be examined.

2. Experimental

2.1. Materials

The membrane substrate was synthesized from PS (Udel P 3500 LCD MP7, MW= 77000, Mn = 22000) using N,N'-dimethylacetamide (DMAc) as a solvent via the phase inversion method. The PA active layer was prepared using 1,3,5-benzenetricarbonyl trichloride (TMC) (>98%) and m-phenylenediamine (MPD) (> 99%) by interfacial polymerization. Hexane was used as the solvent for preparing the TMC solution, and distilled water was used as the solvent for the aqueous phase reactant. All chemicals were purchased from Sigma–Aldrich. The potassium persulfate–sodium metabisulfite (Merck) was used in the redox polymerization system, and acted as the initiator in the grafting process. Methacrylic acid monomer was also supplied by Sigma Aldrich. Zinc acetate was used to synthesize the ZnO nanoparticles. Sodium hydroxide (NaOH; 98%; purchased from El Motaheda) was used for pH adjustments, and sodium lauryl sulphate (SLS) was used as a surfactant. Sodium chloride (NaCl) was used as a representative solute for salt rejection measurements

2.2. Synthesis and characterization of ZnO nanoparticles

The ZnO nanoparticles were synthesized using the hydrothermal method, which does not require the use of organic solvents, and can be considered an environmentally friendly technique [30].

Three grams of zinc acetate was dissolved in 20 ml of distilled water. 16 ml of a 5 M NaOH solution was added drop wise to the zinc acetate solution while gently stirring for a period of 10 min at 90°C (see Eqn 1). During this period, 1.5 g of SLS was dissolved in 15 ml of distilled water and was added to the zinc acetate mixture. SLS, as a surfactant, plays an important role in the modification of the ZnO particles, and acts as an insulator between the nanoparticles, allowing them to overcome the interacting forces between them to create a homogeneous dispersion. A white precipitate appears immediately upon mixing the zinc acetate solution. The mixture was moved to a Teflon stainless steel autoclave (volume 80 ml) and filled with deionized water up to 80% of the reactor volume for hydrothermal treatment at 120°C for 5 h. The autoclave was then allowed to cool down naturally. The suspended ZnO nanoparticles were centrifuged at 6000 rpm for 15 min and collected as a white precipitate. The precipitates were washed with distilled water and ethanol to remove impurities. They were then dried at 50°C for 5 h, and stored.

$$Zn(CH_3CO_2)_2 + 2NaOH \xrightarrow{\Delta\ Tempreature} ZnO + H_2O + 2NaCH_3CO_2 \qquad (1)$$

2.3. Preparation of PA(TFC) and surface modification by ZnO nanoparticals incorporated with grafting (MAA) membranes

The schematic diagram of the membrane fabrication process is shown in Figure 1. The surface grafted PMAA-g-PA(TFC) and the ZnO modified PMAA-g-PA(TFC) membranes were synthesized as described below.

The microporous PS substrate was prepared by the phase inversion method. The PS membrane was cast from a homogeneous polymer solution containing 15 wt. % PS and 85 wt. % DMAc, using a thin film applicator (casting thickness 200 μm) on a horizontal smooth plate. The PA(TFC) membrane was prepared through interfacial polymerization between MPD (2 wt. %) and TMC (0.5 wt. %) on the surface of a PS support layer. Finally, the resulting PA(TFC) membrane (compound II, Figure 1) was thoroughly washed and kept in distilled water for surface grafting and ZnO NP modification.

The schematic diagram of the graft polymerization of MAA on the surface of the PA(TFC) membrane is shown in Figure 1. The PA(TFC) membrane surface has carboxylic acid and primary amine groups on the chain ends. The hydrogen atoms on the end groups and the hydrogen in the amide bond present possible grafting sites for surface modifications via the redox grafting system. The grafting polymerization was carried out with an aqueous solutions of MAA (2.0 wt. %). The redox grafting system, composed of potassium persulfate $K_2S_2O_8$ (1.5 wt. % of monomer) and sodium metabisulfite $Na_2S_2O_5$ (0.33 wt. % of $K_2S_2O_8$), was used to generate radicals. The aqueous solution containing MAA, $K_2S_2O_8$, and $Na_2S_2O_5$ was added to the active PA(TFC) surface layer for 30 minutes at 25 °C without shaking. The PA(TFC) membrane has to be fixed in circular glass frames to ensure contact between the reactant solution and the membrane layer. The resulting PMAA-g-PA(TFC) membrane (compound III, Figure 1) was removed from the frames and washed thoroughly with distilled water several times, and kept in distilled water for testing and characterization.

To prepare the ZnO modified PMAA-g-PA(TFC) membrane different amounts of synthesized ZnO NPs (0.005, 0.05, 0.1, 0.2, 0.3, 0.4 as a wt. % of MAA monomer concentration) were dissolved with an aqueous solutions of the MAA (2.0 wt. %), $K_2S_2O_8$ (1.5 wt. % of monomer) and $Na_2S_2O_5$ (0.33 wt. % of $K_2S_2O_8$) in an ultrasonic bath at 30-40 °C for at least 3h to facilitate the dispersion of the ZnO NPs. The aqueous solution was added to the active PA(TFC) surface layer for 30 minutes at 25 °C without shaking. The resulting ZnO modified PMAA-g-PA(TFC) membrane was removed from the frames and washed thoroughly with distilled water several times and kept in distilled water for testing and characterization. The resulting ZnO NPs modified PMAA-g-PA(TFC) membrane is shown in Figure 1. The schematic diagram in Figure 1 illustrates that the incorporation of the ZnO NPs, with grafting MAA, onto the surface of a polyamide thin film composite membrane PMAA-g-PA(TFC) could have been established through one of two processes. Firstly, the impact of moisture and humidity may have led to the creation of hydroxyl groups on the surfaces of the ZnO NPs, so that, a covalent bond formed through the chemical reaction of the COO- group of PMAA and the ZnO NPs -OH group [13]. The second possible process is the creation of a H-bond between the surface hydroxyl groups of the ZnO NPs, and the oxygen in the COO- group of PMAA [14].

To investigate the impact of ZnO NPs modification on the water flux, salt rejection, bio anti-fouling and mechanical properties, the results obtained from the ZnO modified PMAA-g-PA(TFC) membranes were compared with the pure PA(TFC) and PMAA-g-PA(TFC) membranes.

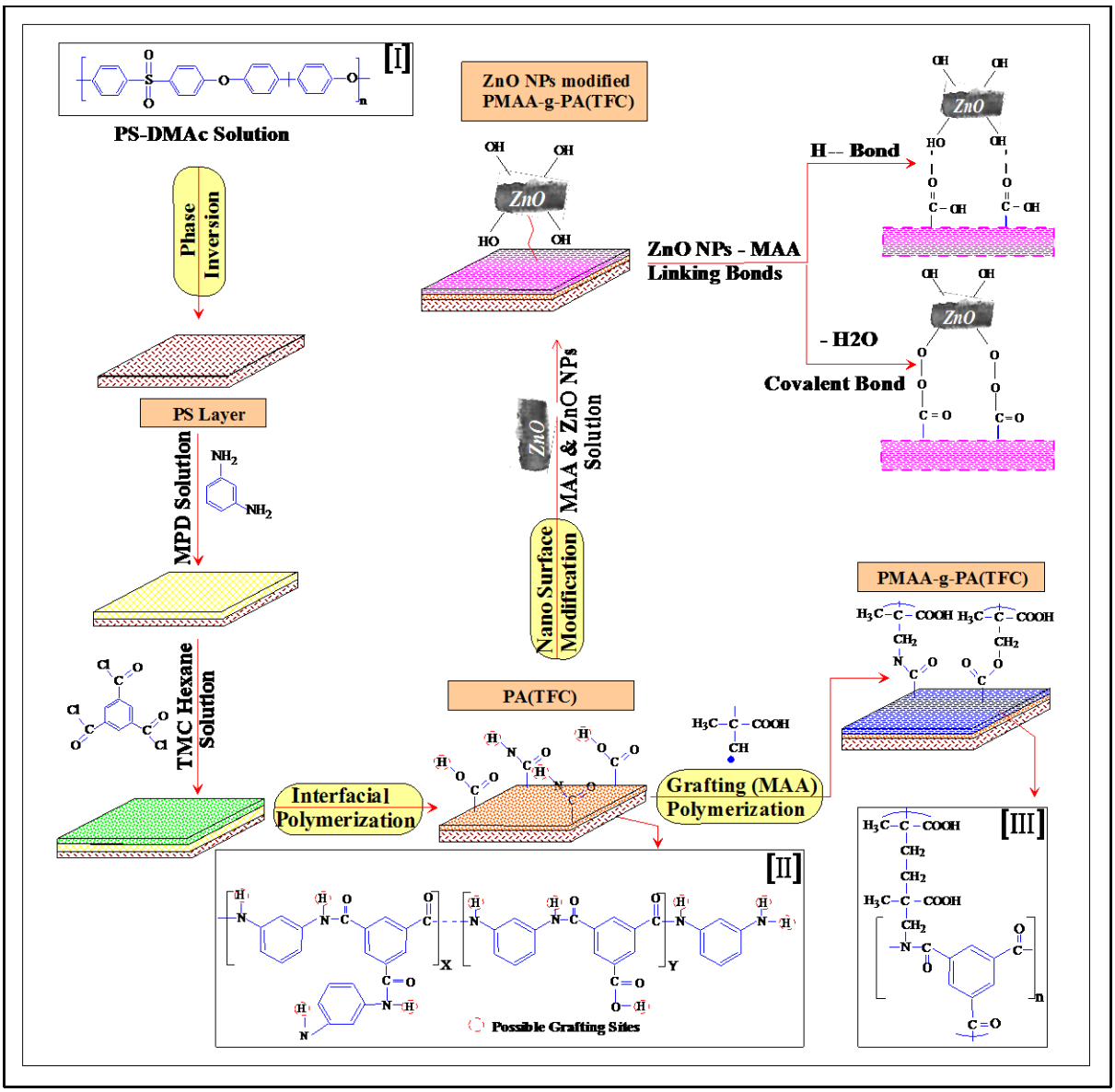

Fig. 1: Schematic representation of PA(TFC) RO membrane, Surface modification via radical grafting polymerization of MAA and surface modification by incorporation of ZnO NPs in the grafting solution.

2.4. ZnO NPs and membrane characterizations and performance assessment

The prepared ZnO NPs were characterized by X-ray diffraction (XRD), transmission electron microscopy (TEM), scanning electron microscopy (SEM) and Fourier transform infrared spectrophotometry (FTIR).

The membranes were characterized by FTIR, X- ray diffraction, SEM, TGA, Mechanical properties and the contact angle. FTIR analysis was carried out using a Gensis Unicam spectrophotometer. The X- ray diffraction patterns of the modified membranes were determined with a Philips Model PW 3710 X-ray diffraction instrument. The scanning electron microscope (SEM, Quanta FEG) was used to visualize the membrane's surface characteristics. To examine membrane cross-sections, membrane samples were prepared by fracturing in liquid nitrogen. Thermal gravimetric analysis was carried out using a Shimadzu TGA system

(TGA-30). The mechanical properties of the membrane samples were measured with Universal Testing Instruments (UTI, V4.5 A, DMA), where the dynamic strain and stress were measured at room temperature (25 °C). Tensile tests were carried out to assess the Young's modulus and strain at fracture of samples at the rate of 10 mm/min. The membrane samples were cut into rectangles with a dimension of 20 x 13 x 0.15 mm, and fixed perpendicular to one another in between two automatic gripping units of the sample, leaving a 3 cm sample extent for mechanical loading. The thickness of the membrane samples was determined with an automatic micrometer with a precision of 1 µm. Young's modulus (Mega pascal, M pa) was calculated using the following equation:

$$\text{Young's modulus (Mpa)} = \frac{\text{Stress}}{\text{Strain}} \qquad (2)$$

The hydrophilicity of the membrane surface was measured using a Tantec contact angle meter at 25°C. A water drop was placed onto the membrane surface with a digital micro syringe with contact angle between the water and the membrane measured when no further change was observed. On average, 8 measurements were obtained for each membrane sample.

The degree of grafting (DG) was evaluated based on weight change per membrane surface area:

$$DG = \frac{(Wm - W0)}{A} \qquad (3)$$

where W_0 is the weight of the initial dry membrane sample, W_m is the dry weight of the membrane after grafting modification, and A is the surface area of the membrane.

The membranes ability to carry out water desalination was judged in terms of salt rejection (SR %) and water flux (Jw, l/m^2.h), using a laboratory DDS reverse osmosis system (model LAB M20, Alfa Laval Denmark). The effective membrane area was 18 cm^2. Pure water flux was measured, followed by a reverse osmosis test with an aqueous NaCl solution of 2000 mg/L. The dissolved salt in the feed and permeate water were measured using a conductivity meter. The measurements of salt rejection and water flux and were taken 30 minutes after filtration to ensure a steady state had been reached. In addition, a groundwater sample, with a total dissolved solid concentration of 35264 mg/L collected from the Miocene aquifer in Sharm El Shiekh, Sinai, Egypt, was used to examine and compare the membranes. The water flux and salt rejection were calculated from the following equations:

$$J = \frac{Vp}{At} \qquad (4)$$

$$R = \left(1 - \frac{Cp}{Cf}\right) \times 100 \qquad (5)$$

Where, J is the water flux (L/m^2h), Vp the permeate volume (L), A the surface membrane area (m^2), t the filtration time (h), R the salt rejection, and Cp and Cf the concentrations of permeate and feed solution, respectively.

The release of zinc ions from the surface structure of the modified membranes was evaluated via batch experiments. In these experiments, the membrane sample was placed in distilled water (DI), where the ratio was 80 cm^2 membrane samples to 20 ml DI water. Samples were left on a shaker (Sk-O180-Pro; 120 rpm), and the DI water was replaced every 24h. The collected water samples were acidified with 1% HNO_3 and analyzed using a Prodigy radial inductively coupled plasma optical emission spectrometer (ICP-OES) (Teledyne-Leeman).

2.5. Antibacterial assessment of PA(TFC), PMAA-g-PA(TFC) and ZnO NPs modified PMAA-g-PA(TFC) membranes.

Pre-cultures of *Escherichia coli* (*E. coli*) cells were prepared in 10 ml of Luria-Bertani (LB) medium (1 wt. % yeast and 1 wt. % NaCl in deionized water) at 37°C for 24 hours. The prepared solution was diluted with purified water, and a dilute solution (20ml, total $670X10^6$ cells) was pipetted onto the prepared membrane surfaces PA(TFC), PMAA-g-PA(TFC), ZnO NPs modified PMAA-g-PA(TFC) membrane. The prepared system was illuminated with a 365 nm UV lamp placed 20 cm over the top of the membrane surface for 90 minutes. A volume of 1 ml of *E. coli* solution was placed on LB agar medium and incubated for 24 hours. The percentage survival of *E. coli* was determined by counting the number of viable cells in terms of colony-forming units (CFU/ml).

3. Results and discussion

3.1 Characterization of the synthesized ZnO NPs

The prepared ZnO nanoparticles were characterized by X-ray diffraction and displayed crystalline structures. As shown in Figure 2a there were three pronounced pure diffraction peaks (100, 002 and 101) at 2θ equal to 32.03°, 34.64° and 36.51°, respectively. These peaks match with the standard data sheets (JCPDS 36-1451) reported by the Joint Committee on powder diffraction, which confirms the formation of zinc oxide in hexagonal shapes [31]. No peaks corresponding to impurities were detected, indicating pure ZnO nanoparticles were obtained.

The average particle size for the nanoparticle powders were deduced using Scherer's equation [32]:

$$d = \frac{0.9\lambda}{\beta \cos\theta} \qquad (6)$$

where λ is the wavelength of the X-ray (1.54 A°), d is the crystallite diameter of ZnO nanoparticles, β is the whole width at half maximum width of the diffraction peak in radiance, and θ is the maximum intensity of the diffraction angle. The crystallite size of the ZnO particles was determined to be between 90 and 144 nm, with an average size of 118 nm. The X-ray diffraction patterns of all investigated materials showed a high degree of crystallinity.

The functional groups of the synthesized ZnO NPs were analyzed using the FTIR spectrum. Figure 2b shows the spectra of Zno NPs in the range of 400-4000 cm^{-1}, at room temperature. A stretching band of Zn–O near 415cm^{-1} was shown. The peaks at 3400- 3500 and 1580 cm^{-1} indicate the presence of hydroxyl (–OH) and carbonyl (C=O) residues, possibly due to atmospheric moisture and CO_2, respectively. The spectroscopic studies indirectly provide information about the surface characteristics of the ZnO NPs, where the small peak appears at approximately 900 cm^{-1}, indicating the Zn–OH has important applications for zinc oxide NPs.

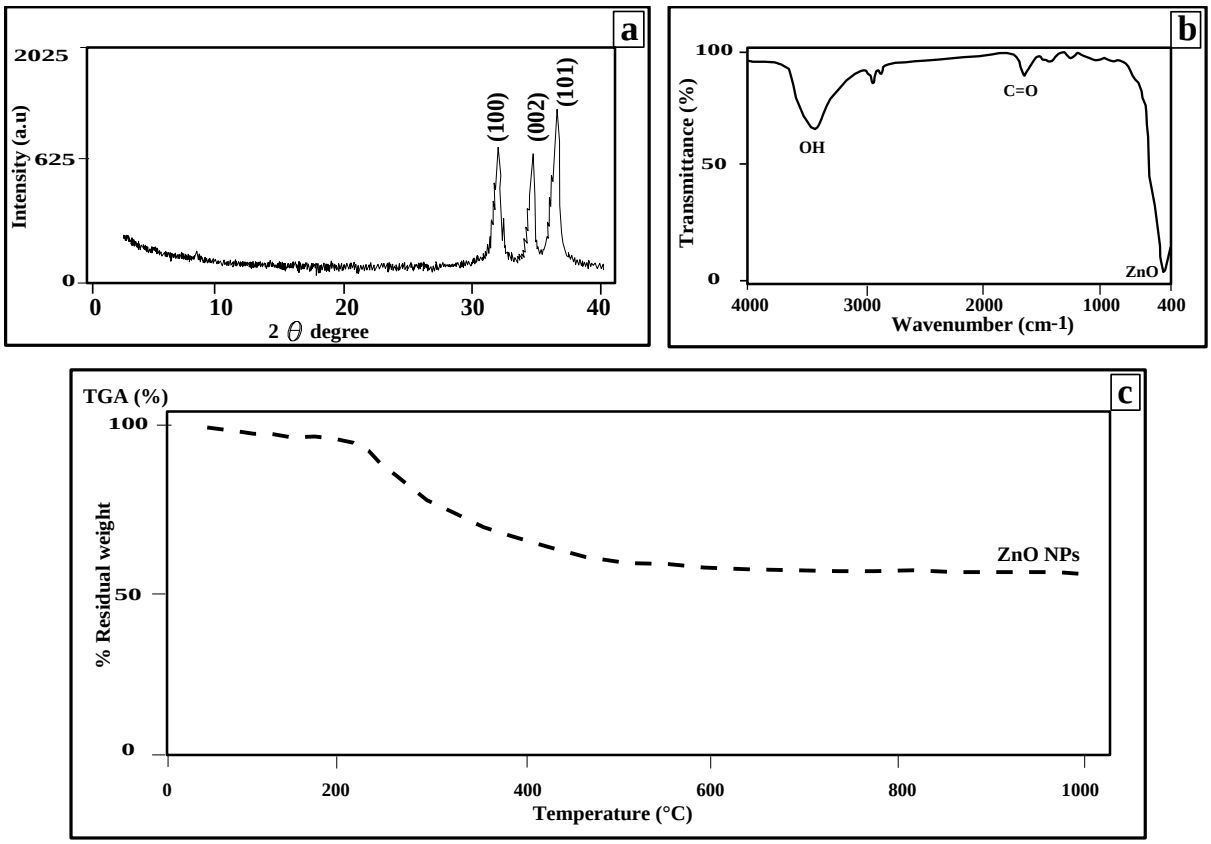

Fig. 2: X-ray diffraction pattern of synthesized ZnO NPs (a), FTIR spectra of synthesized ZnO NPs (b) and thermal analysis curves for the obtained samples of ZnO NPs (c)

The thermal properties of the pure ZnO NPs were investigated using TGA analysis, which provides information on the chemical and physical transformations and thermal stabilities upon heating. TGA analysis of ZnO NPs show that weight loss proceeds in successive stages, with increasing temperature. In Figure 2c, the TGA graph shows successive weight loss up to 500°C, and after this point there was no significant weight loss detected. The first weight loss occurred at 125°C, representing the dehydration of samples due to desorption of physically adsorbed water molecules on the ZnO NP surface [33]. The second step, possessing the greatest mass loss, occurred between 200 and 350 °C, indicating the loss of OH^- and CO_3^{2-}.

The surface morphology of the ZnO NPs was characterized by scanning electron microscopy (SEM). In Figure 3a,b the ZnO nanoparticles appear in rod shapes, with smooth surfaces and a size range around 100-160 nm.

The TEM image was used to characterize the shape and size of the synthesized ZnO NPs. The results are shown in Figure 3 c where the ZnO NPs appear as straight, elongated, smooth rods. The diameter and the length of the nanoparticles ranged from 10–20 and 50–100 nm, respectively, with an average of 44 nm. The size range presented here is close to the previous dimensions obtained from the SEM, and grain size range from the XRD. Furthermore, the chemical reactivity of the nanoparticles tends to be enhanced as a result of decreasing particle size due to an increase in the surface to volume ratio.

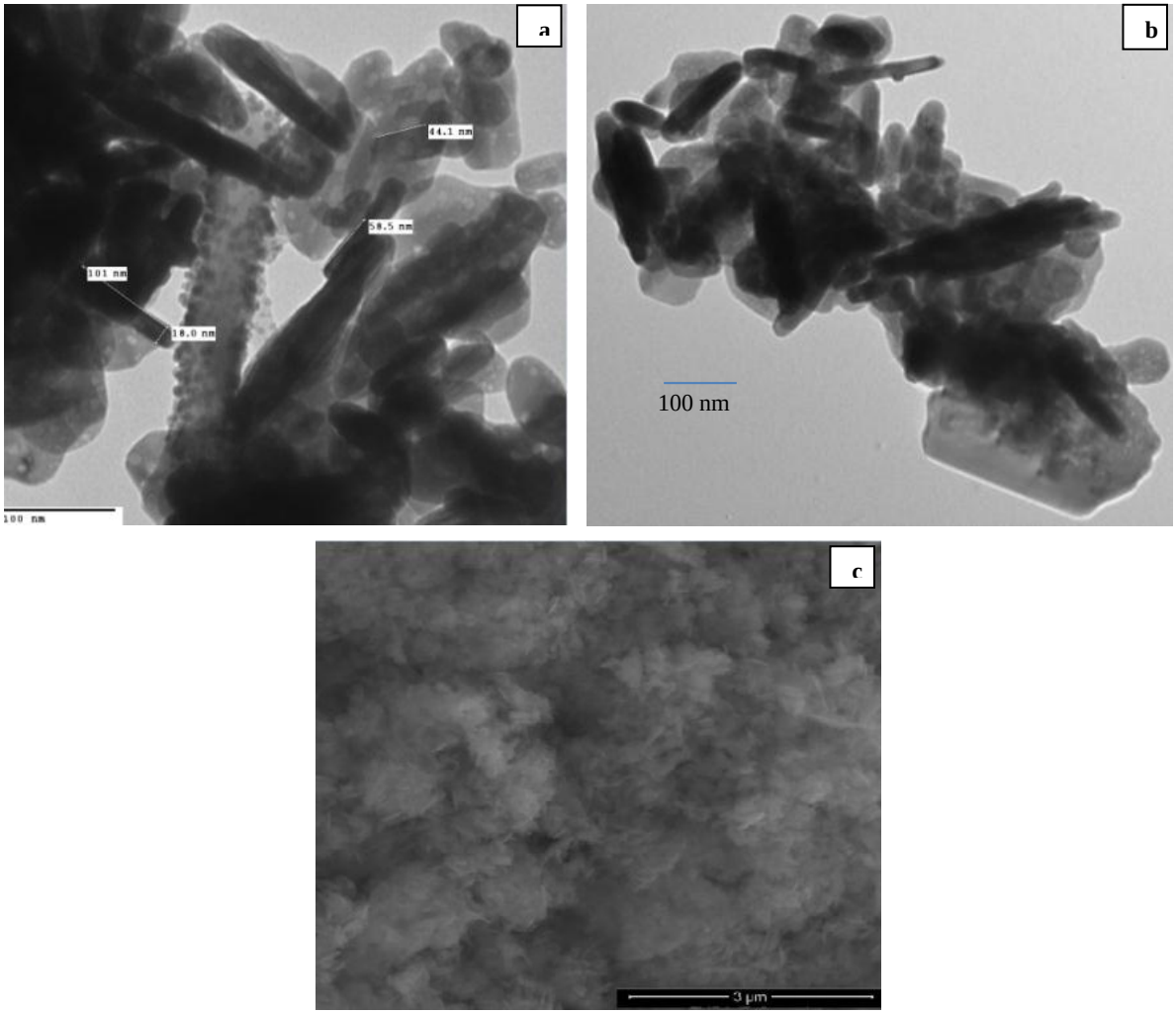

Fig. 3: SEM images of ZnO NPs (a,b) and TEM image of the ZnO NPs (c).

3.2. Membrane characterization

3.2.1. FTIR spectroscopy:

FTIR spectroscopy can provide a convenient and effective way to determine the functional groups of the modified and unmodified thin film composite RO membranes. FTIR was performed to confirm the successful preparation of PA(TFC) membranes onto the PS support layer, to verify the successful graft polymerizations of PMAA onto PA(TFC) membranes, and to determine the functional groups in the ZnO NPs modified PMAA-g-PA(TFC) membrane.

Figure 4a shows the characteristic peaks of both the PS support layer and the PA(TFC) membranes. The FTIR shows a peak band appearing at ~708 cm^{-1} due to the C–H bond in the aromatic group. The band at ~866 cm^{-1} is caused by the hydrogen deformation of para substituted aryl groups [34]. The band at 1265 cm^{-1} is representative of an asymmetric stretching vibration of the C–O–C in the aromatic ether group. The FTIR shows two bands around ~1327 which can be attributed to a symmetric stretching vibration of O=S=O, corresponding to pure PS [35]. The observed band around ~1597 cm^{-1} is mainly attributed to the rotation of the C=C of the benzene ring.

The PA(TFC) spectrum is used to confirm whether the interfacial polymerization has occurred (Figure 4a).The appearance of two bands around 1600 cm^{-1} and 1265 cm^{-1} for the C=O stretching vibration and C-N group of the amide II on PA(TFC) membrane, respectively [36]. The spectrum reveals that there is a band around 1500-1540 cm^{-1} that is related to the N–H (amide II) in-plane bending [37], or possibly a C-N stretch [38]. The new band appearing at ~1743 cm^{-1} corresponds to the stretching of (C-OH) in the carboxylic group (O=C–OH). The peak at 1460 cm^{-1} represents the C=O stretching and O–H bending of carboxylic acid [39,40]. Also, the stretching peak at 3377–3482 cm^{-1} can be assigned to N–H and O–H, and suggest successive destructive structures associated with the interfacial polymerization of the PA(TFC) membrane [41].

The FTIR spectra of the PMAA-g-PA(TFC) structured membranes indicate the presence of carboxylic acid groups. The peak shifts at ~1610 cm^{-1} in Figure 4a corresponds to linking of the MAA with the C=O group of carboxylic acid, incorporated in the PA(TFC) membrane [42] as indicated in Figure 1. The C=O in the amide group stretched to a lower frequency peak (~1583 cm^{-1}) forming hydrogen bonds with N-H groups at the possible grafting sites on the PA(TFC) membrane surface Figure 1. The new band, located at ~1770cm^{-1}, and representing the appearance of the carbonyl (C=O) group is mainly attributed to the dimers of MAA [43]. Peaks appearing between the band range of ~2890 to ~3000 cm^{-1} correspond to $–CH_2$ and $–CH_3$ stretching vibrations from PMAA. The PMAA grafting process takes place at the possible grafting sites of –HO and –NH groups assimilated in the chemical structure of the PA(TFC) membrane compound I, indicated in Figure 1. The FTIR spectrum of the PMAA-g-PA(TFC) show that all bands of –HO and –NH have been merged into one line, constructing a large peak plateau between ~3158-3500 cm^{-1} Figure 4a. The construction of this plateau is normally associated with a Stretching vibration and banding shift of –OH and –NH due to the development of the PMAA-g-PA(TFC) compound II, Figure 1.

The spectrum of the ZnO NPs modified PMAA-g-PA(TFC) membrane is shown in Figure 4a. Comparing the ZnO NPs modified PMAA-g-PA(TFC) membrane with the pure PA(TFC) membrane illustrates that there is a stretching vibration band that appears at approximately 1596 cm^{-1}. This band is most largely caused by COO-Zn, representing the covalent bond between the –COOH [13] group of the MAA and the hydroxyl (–OH) group on the surface of the ZnO NPs Figure 1 and 4a. The appearance of the hydroxyl (–OH) group peak around 3480 cm^{-1}, is due to the formation of the intramolecular hydrogen bond [14] between the carboxylic groups (COO-) of MAA and the hydroxyl group on the surface of the ZnO NPs Figure 1. The PMAA is flexible, and the hydroxyl groups on the surface of the ZnO NPs can easily find a carbonyl group to form the hydrogen bond that will be stabilized on the membrane surface. The stretching vibration peak, appearing at ~ 1770 cm^{-1}, is mainly attributed to the dimers of MAA. The incorporation of ZnO NPs into the MAA grafting solution is inferred by the shift of the carboxylic peak due to electron acceptance from the Zn atoms [44]. This shift is due to the interaction between the carboxylic groups (COO–) contained in the MAA and the ZnO NPs [45]. Finally, these peaks indicate the successful incorporation of ZnO NPs on the surface of the PMAA-g-PA(TFC) membrane.

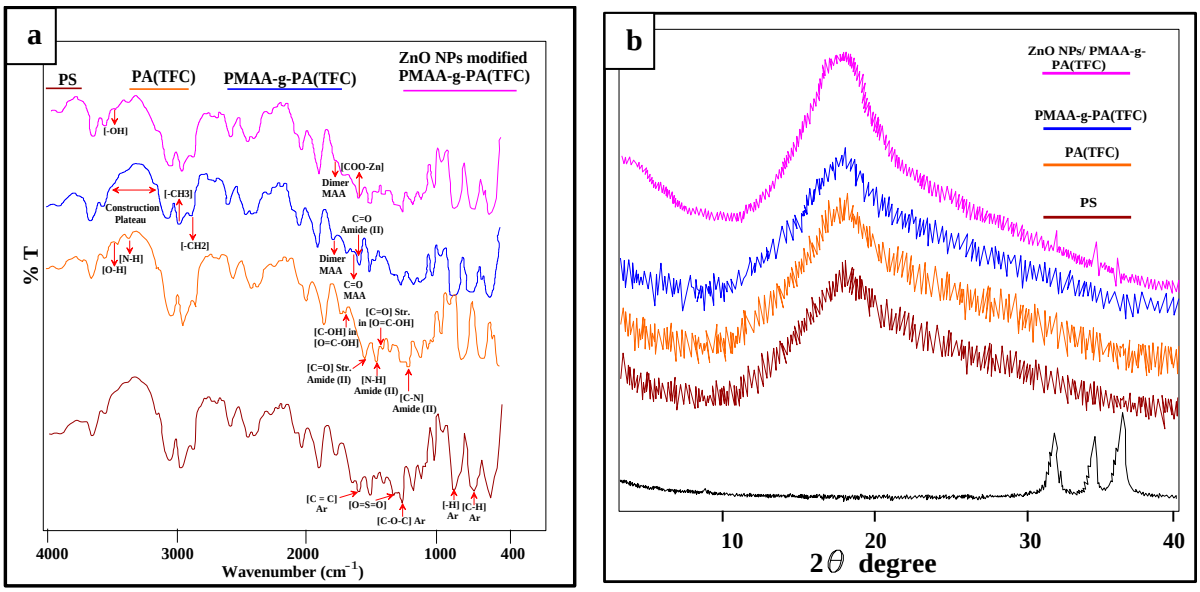

Fig.4: Spectrum analysis of membrane surface: (a) FTIR, (b) X-ray diffraction pattern

3.2. 2. X-ray diffraction patterns

The X-ray diffraction (XRD) technique was used to investigate the change in the crystalline and noncrystalline nature of the PS and the PA(TFC) membranes and to elucidate the structure pattern between the PMAA-g-PA(TFC) and ZnO NPs modified PMAA-g-PA(TFC) membranes and that may occur during grafting with the PMAA, as well as after incorporation of the ZnO NPs into the membrane. In Figure 4b, the PS, PMAA-g-PA(TFC) and PMAA-g-PA(TFC) membranes are completely amorphous in nature, and do not show any sharp diffraction peaks. In Figure 4b, the dominant peaks of ZnO NPs appear at 2θ angles of 32.03^{o}, 34.64^{o} and 36.51^{o}. The ZnO NPs modified PMAA-g-PA(TFC) membrane shows the same crystalline characteristic peaks at 2θ angles in analog to the main characteristic peaks of ZnO NPs. The XRD results show that nanoparticles remain in the grafting layer of the membrane surface; however, all characteristic peaks in the grafting layer were shifted to slightly lower angles compared with those of ZnO NPs. This shift may be due to slight interactions between ZnO NPs and the MAA on the modified grafting layer, possibly indicating that a small amount of ZnO NPs is consumed to form a poly(zinc methacrylate) complex on the surface of the PA(TFC) membrane.

3.2.3. Morphology analysis of membranes

SEM was used to observe the surface and cross sectional morphology of each membrane, including PS, PA(TFC), PMAA-g-PA(TFC) and ZnO NPs modified PMAA-g-PA(TFC) membrane. Figure 5a shows the PS support layer is porous, with a nano metric pore size, and a smooth surface. Figure 5b shows the surface of a PA(TFC) layer, where a dense structure containing nodules typical of PA films was observed. The PMAA-g-PA(TFC) grafting shows nodules, and the pore size was found to increase with an increase in grafting reaction Figure 5c. Additional ZnO NPs in the grafting solution lead to rougher membrane surfaces, with some aggregation of ZnO NPs Figure 5d. It is apparent that the ZnO NPs are uniformly dispersed along the membrane surface, which exhibits increased pore density and pore size. It is believed that the addition of ZnO NPs improves the membranes surface properties and generates new flow paths through the membrane layer, causing an increase in water sorption and permeability.

Cross- sectional observations of the membranes were also made under SEM Figure 5e. The cross sections of the porous PS layer before the interfacial polymerization show a spongey, nodular, finger–like structure of 124 µm thickness. The nodular shapes detected near the surface of the PS layer are tightly compacted, submicron in size Figure 5e, and covered by the PA layer in the (TFC) membrane Figure 5f. A closer SEM examination of the PA PS layer reveals a thin PA layer of about 1 µm in thickness penetrating the top of the PS layer. As shown in Figure 5g, the PMAA-g-PA(TFC) membrane displayed a pore-like structure on the membrane surface, which was improved by the grafting layer. The sponge- like structure is more pronounced at a higher grafting degree.

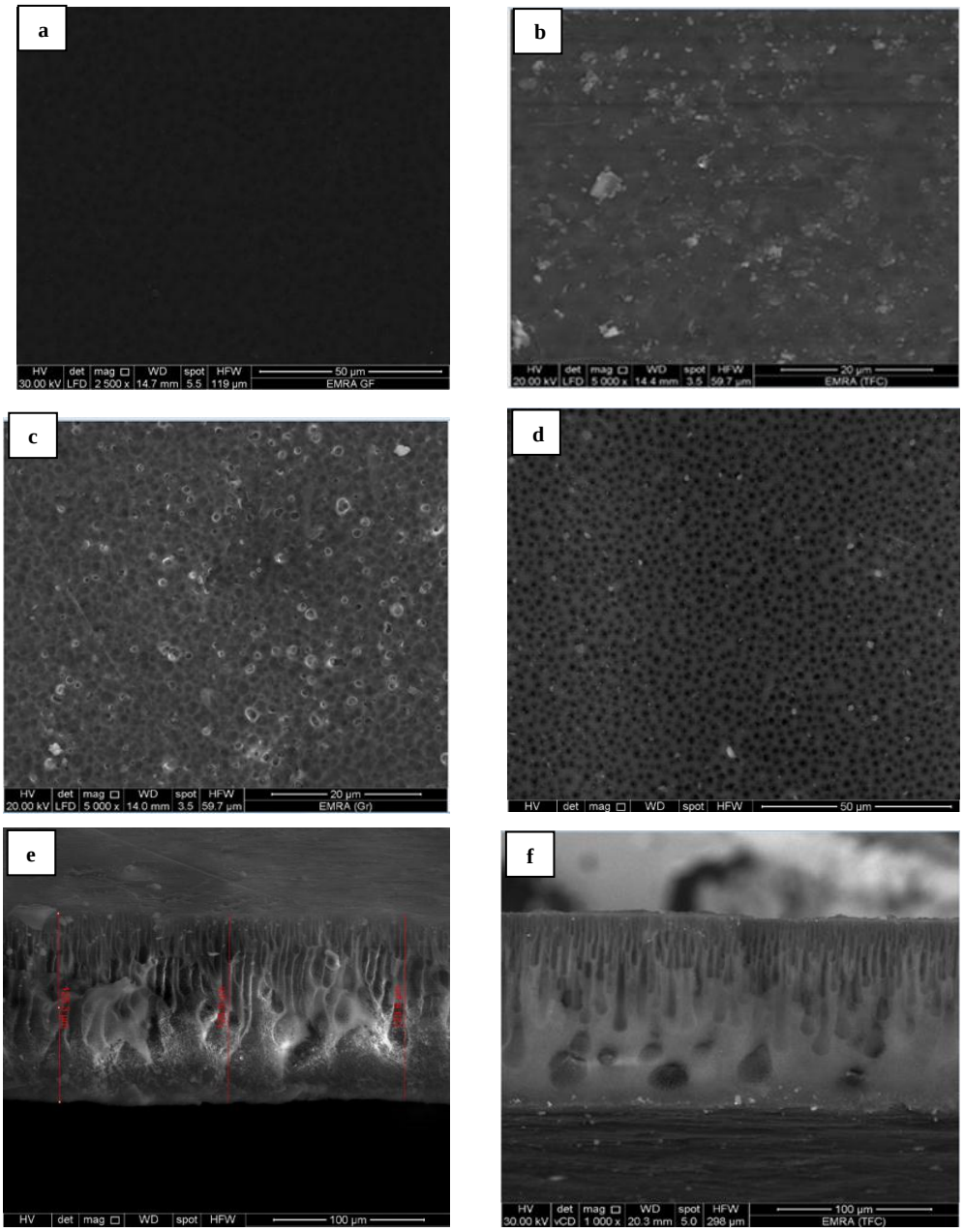

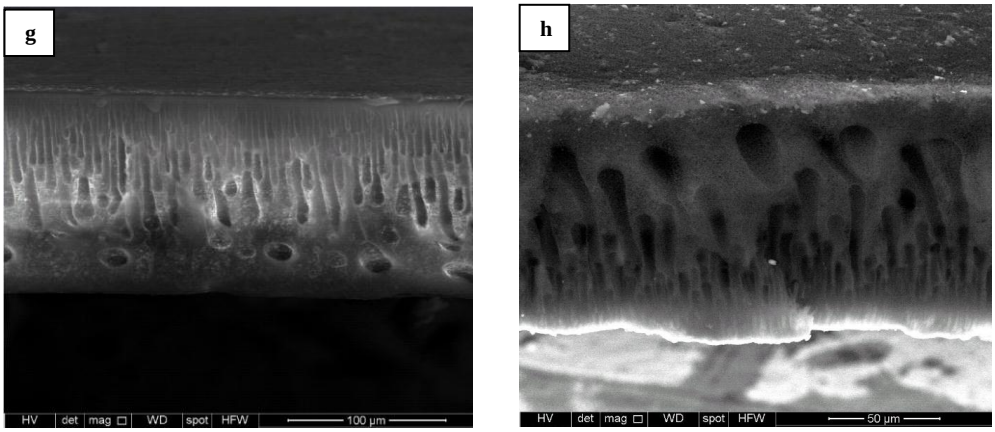

Fig. 5: SEM images of Top surface for a) PS, b) PA(TFC), c) PMAA-g-PA(TFC) and d) ZnO NPs modified PMAA-g-PA(TFC) membranes and images e, f, g and h are SEM cross sections for the same membranes, respectively.

The ZnO NPs, possessing the grafting solution on top of the PA(TFC) membranes, showed small, irregular, finger-like structures with clusters of ZnO NPs on the surface of the PA(TFC) membranes Figure 5h. A homogeneous propagation of the nanoparticles in the polymer matrix is shown on the surface, and there is little evidence of ZnO NPs agglomerations near the surface of the PA(TFC) membrane. ZnO NPs modified PMAA-g-PA(TFC) and PMAA-g-PA(TFC) membranes show smooth, homogeneous surfaces, and seemingly large porosity with less porous voids near the surface. These enhancements in the membrane surface lead to new flow paths in the membrane layer allowing increased water permeability and sorption.

3.2.4. Mechanical properties of the synthetic membranes:

The mechanical properties of PS, PA(TFC), PMAA-g-PA(TFC) and ZnO NPs modified PMAA-g-PA(TFC) membranes are shown in Table 1, and the stress-strain curves are shown in Figure 6. The PMAA-g-PA(TFC) and ZnO NPs modified PMAA-g-PA(TFC) membranes show improved tensile strength (Mpa), elongation break (%), and significantly increased Young's modulus values when compared to the PS and pure PA(TFC) membranes. The membranes possess tensile strength values in the following order: ZnO NPs modified PMAA-g-PA(TFC)> PMAA-g-PA(TFC)> PS > PA(TFC) membranes, while the order for elongation break and Young's modulus was: ZnO NPs modified PMAA-g-PA(TFC)> PMAA-g-PA(TFC)> PA(TFC)> PS membranes. The improvement in tensile strength values for the PMAA-g-PA(TFC) membrane is mainly due to the cross-linked network structure in the alkyl group, and the rigid aromatic structure in the membrane backbone Figure 1.

The mechanical properties of the ZnO NP modified PMAA-g-PA(TFC) has been enhanced by the addition of a reduced amount (0.1 wt. %) of ZnO NPs onto the membrane surface, causing increased strength and flexibility. The mechanical properties of the membrane depend mainly on the membrane microstructure and intermolecular forces operating along the membrane backbone [46]. Also, the addition of ZnO NPs to the membrane makes it more crystalline, and the crystalline membrane is stronger than the amorphous ones.

The addition of small amounts of ZnO NPs to the membrane surface causes a uniform dispersal of ZnO NPs in the membrane matrix. This dispersal provides higher uniform stress distribution, reduced creation of

stress-concentration centers, and consequently enhances the mechanical properties of the membrane [47]. Furthermore, the linkage bond between the ZnO NPs and MAA on the surface of the PA(TFC) membrane creates flexible spacers on the nanoparticle-membrane interface, which enhances the rigidity of the membrane chain.

These results indicate that, ZnO NPs modified PMAA-g-PA(TFC) membranes with reduced ZnO NPs content had random dispersal, and showed less agglomeration in the membrane matrix, thus creating membranes with superior mechanical properties.

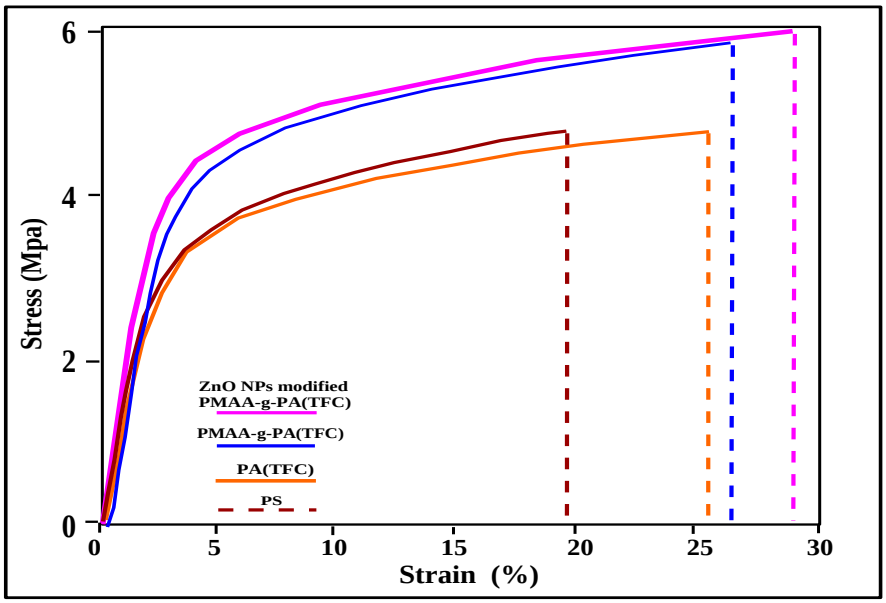

Fig. 6: The mechanical properties of PS, PA(TFC), PMAA-g-PA(TFC) and ZnO NPS modified PMAA-g-PA(TFC) membranes.

Table (1): Mechanical properties of PS, PA(TFC), PMAA-g-PA(TFC) and ZnO NPS modified PMAA-g-PA(TFC) membranes.

Membrane type	Tensile strength (Mpa)	Maximumelongation (%)	Young's modulus (Mpa)
PS	4.85	19.5	0.89
PA(TFC)	4.8	25.2	0.89
PMAA-g-PA(TFC)	5.83	26.6	1.09
ZnO NPs modified PMAA-g-PA(TFC)	6	29	1.23

3.2.5. Hydrophilicity of the membranes:

The water contact angle (θ; CA) is the most common parameter used to describe the hydrophilicity of membrane surfaces. Hydrophilic membranes possess a contact angle of $0° < \theta < 90°$, while hydrophobic membranes have a contact angle of $90° < \theta < 180°$. In Figure 7, the mean water contact angles for the PS, PA and

PMAA-g-PA(TFC) membranes were 71 ± 2.8°, 66 ± 2°, and 63 ± 2.5°, respectively, indicating they possess hydrophilic surfaces. The high hydrophilicity of the PMAA-g-PA(TFC) membrane is mainly attributed to the presence of the carboxylic group formed as a result of the grafting of MAA, which retains a less negative charge on the membrane surface. The ZnO NPs modified PMAA-g-PA(TFC) membrane show a lower contact angle of approximately 50 ± 3° at room temperature, suggesting that the surface hydrophilicity increased with surface modifications.

The improved hydrophilicity of the ZnO NPs modified PMAA-g-PA(TFC) membrane may be due to a greater attraction of water molecules by the nanoparticles, and to the presence of active hydrophilic functional groups on the membranes surfaces. The CA decreased upon addition of the ZnO NPs causing an increase in the surface energy. This increase in surface energy allows water to easily spread onto the surface and increases the capability of the hydrophilic pores to imbibe water via capillary effects. The surface hydrophilicity of the membrane also helps to improve the antifouling properties [48].

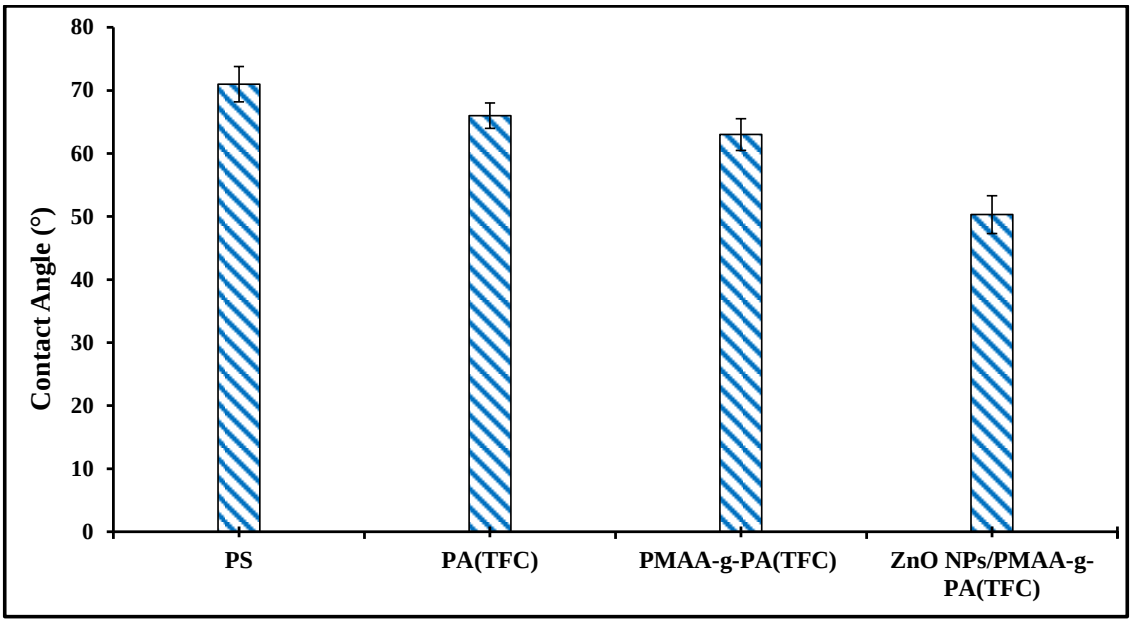

Fig. 7: Contact angles measured on the surface modification membranes.

3.2.6. Thermal stability of the membranes

Thermo-gravimetric analysis (TGA) was performed for PS, PA(TFC), PMAA-g-PA(TFC), and ZnO NPs modified PMAA-g-PA(TFC) membrane membranes under a nitrogen atmosphere, as shown in Figure 8. The TGA curves for all membranes shows that below 500 °C the observed change in weight loss (%) was slow. When the temperature reaches 500-600 °C, weight loss (%) happens rapidly because of the decomposition of PS into CO_2 and H_2O [49]. In both PS and pure PA(TFC) membranes, there are two stages of weight loss observed in the TGA curve Figure 8. The first stage, between 451–561°C and 304–551°C for the PS and the PA(TFC), respectively, was largely caused by the splitting of the sulfonic acid groups $–SO_3H$. The second stage, between 700 °C and 760 °C, was related to the splitting of the polymer main chain. It is notable that the S=O group in the main chain of the PS seems to form an intermolecular hydrogen bond with water. A weight loss in pure PA(TFC) membranes above 760 °C is related to the splitting of the carbon atoms at more than 600 °C. The

thermal stability of the PA(TFC) membrane is due to its ideal chemical structure, which is composed of amide groups and aromatic benzene rings, generally known to be highly resistant to increases in temperature.

The TGA of PMAA-g-PA(TFC) membranes reveals an increase in thermal stability with an increase in the surface modification of the PMAA grafting layer, possibly attributable to the higher thermal stability of PMAA. The weight loss at the first stage of the PMAA grafting layer is interpreted as the release of water (10%). The increase in weight loss is attributable to the decarboxylation reaction of the grafted acid. The TGA curve of ZnO NPs modified PMAA-g-PA(TFC) membrane shown in Figure 8 indicate that thermal degradation was shifted to a higher temperature than pure PMAA-g-PA(TFC). The first weight loss, between 500-630°C, is mainly due to the binding water, lower molecular weight compounds and initiator residuals fragments [50]. The second weight loss, between (630-710 °C), corresponds to PMAA decomposition to carbon monoxide, carbon dioxide. The TGA results show that the incorporation of ZnO NPs significantly enhances the thermal stability of the PMAA–g-PA(TFC) membrane, resulting in an increase of approximately 50 °C, where, the incorporation of ZnO NPs strengthened chemical bonds within the polymeric backbone.

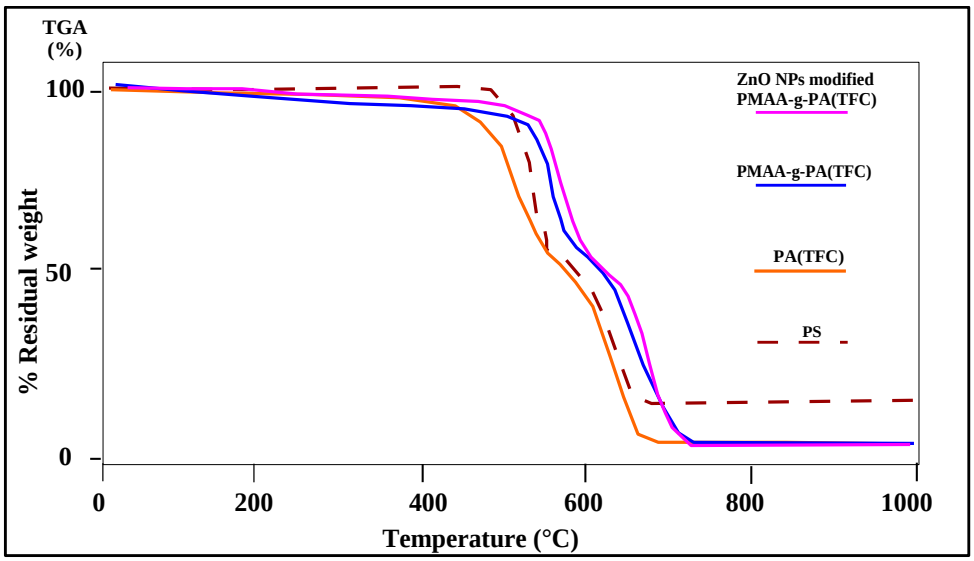

Fig. 8: TGA curves of PS, pure PA(TFC), PMAA–g-PA(TFC) and ZnO NPs modified PMAA–g-PA(TFC) membranes with the heating rate of 10°C/min.

3.2.7. Performance evaluation

The main goal of this research is to introduce a new functional group using grafting processes, thereby improving the membrane surface structure through incorporation of ZnO NPs. This incorporation leads to enhanced membrane performance for water desalination.

Figure 9a shows the water flux and salt rejection for a feed solution of 2000 mg/L NaCl at an applied pressure of 15 bars and a temperature of 25°C. The grafting polymerization of the PMAA-g-PA(TFC) membrane showed improved water flux and salt rejection for the PA(TFC) with increasing MAA monomer concentrations (0.1 to 2 %). Improved water flux and salt rejection may be due to increased grafting degree, which enhances the hydrophilicity and causes negatively charged membrane surfaces [51]. Further increasing

the MAA monomer concentration, beyond 2%, causes a decline in water flux and salt rejection, where, intense polymerization processes produce a dense membrane with low porosity.

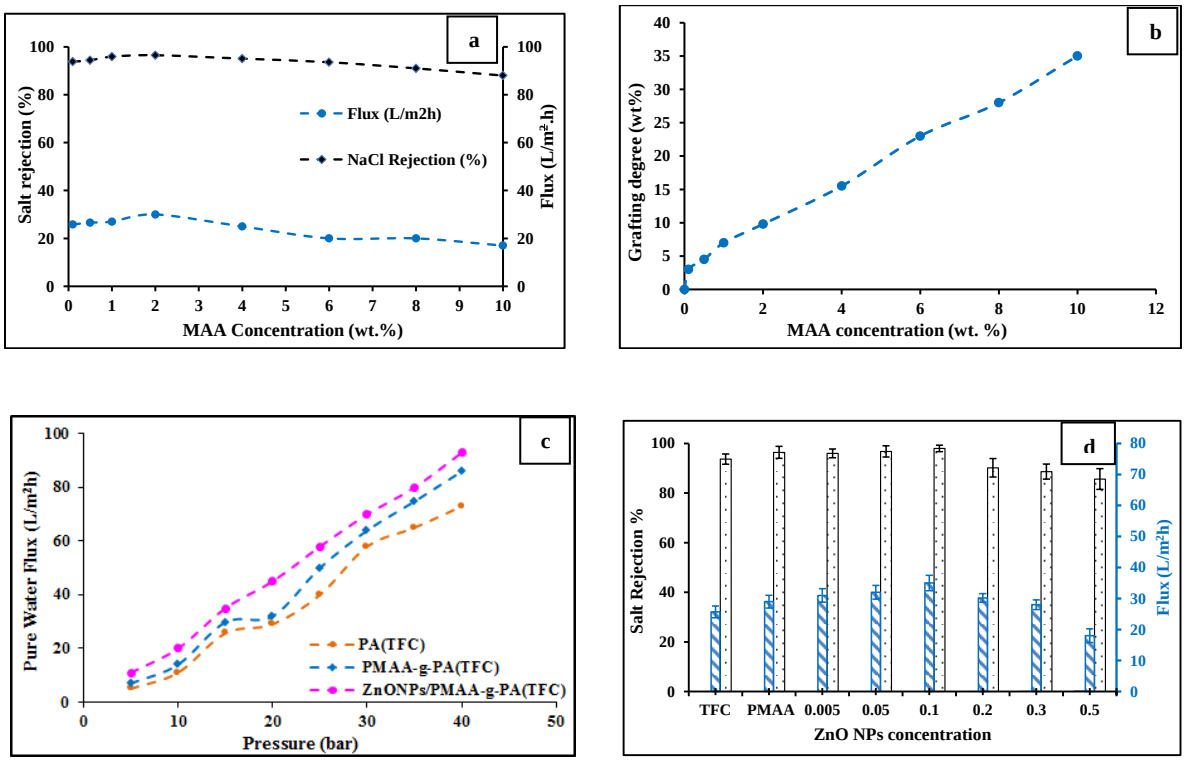

Fig. 9: Performance of membrane samples: (a) Effect of MAA content in aqueous solution on salt rejection and water flux of the resulting PA(TFC) membrane testing with 2000 mg/L NaCl aqueous solution at 15 bar, 25°C ($K_2S_2O_8$ = 1.5 wt. % ; $Na_2S_2O_5$ = 0.333 wt. % of $K_2S_2O_8$; reaction time = 30 min. and reaction temperature = 20°C); (b) The effect of monomer concentration on grafting degree; (c) Pure water permeability at different applied pressures; (d) Flux and salt rejection with increasing weight of added ZnO NPs (2000 mg/L NaCl solution was fed under 15 bar and 25°C) for the prepared membrane.

The effect of MAA monomer concentrations on the grafting degree was examined under the same conditions of initiators, pressure, time and temperature. In Figure 9b, the degree of grafting (%) increases with the MAA concentration from 0.1 to 10% in aqueous solutions. This is mainly attributable to the increase in the number of monomer molecules accessible to react with the free radical initiator incorporated in the PMAA main chain. The degree of membrane grafting is directly proportional to the concentration of MAA monomers, and tends to facilitate the determination of the optimum grafting degree of the proposed application.

Figure 9c shows the pure water permeability for all membranes under pressures ranging from 10 to 40 bars. The ZnO NPs modified PMAA-g-PA(TFC) membrane (0.1 % ZnO) shows comparable water permeability to the other two membranes, with a PWP value of 93 L/m^{2}h at 40 bars. The improved PWP values for the ZnO NPs modified PMAA-g-PA(TFC) membranes are due to the modified grafting layer. This change promotes membrane permeability and attracts water molecules that pass through the membrane matrix and enhance water flux. The addition of ZnO NPs also results in an increase of membrane hydrophilicity, which positively promotes water flux and pure water permeability [52].

In addition, the performance of the membranes with different concentrations of ZnO nanoparticles has been investigated. The water flux and salt rejection for the PA(TFC), PMAA-g-PA(TFC), and modified PMAA-g-PA(TFC) with ZnO NPs concentrations ranging from 0.005 to 0.5 at a feed pressure of 15 bars and a temperature of 25 °C are shown in Figure 9d. The ZnO NPs modified PMAA-g-PA(TFC) membrane showed superior water flux and salt rejection than the pure PA(TFC) and PMAA-g-PA(TFC) membranes. An optimum membrane performance was obtained at 0.1 wt. % of the ZnO nanoparticles. The water flux increased from 31 to 35 $L/m^2.h$, while the salt rejection increased from 96.6 to 98%, with an increase in ZnO nanoparticle concentration from 0.05 to 0.1 % of the total membrane weight. Beyond a ZnO NPs concentration of 0.1 wt. %, the membrane performance declined with increasing ZnO concentrations.

3.2.8. Membrane application and groundwater desalination

The fabricated membranes have been tested using the reverse osmosis pilot-scale laboratory unit (Unit M20) to investigate the membrane desalination performance and assess salt rejection. A groundwater sample, collected from the Miocene aquifer in Sharm El Shiekh, Sinai, Egypt, was used as a feed source in the RO pilot-scale unit using the prepared sheets of PMAA-g-PA(TFC) and ZnO NPs modified PMAA-g-PA(TFC) membranes. The feed groundwater and the desalinated product water were analyzed for major ion constituents to determine the efficiency of the membranes under constant pressure (30 bar), temperature (25°C) and flow rate (5 L/min). The initial groundwater salinity and major ion concentrations are illustrated in Table 2. Figure 10 shows that the salt retentions of bivalent ions are higher than that of monovalent ions for cations and anions using both membranes. Thus, the salt rejection (TDS in mg/L), using the PMAA-g-PA(TFC) and ZnO NPs modified PMAA-g-PA(TFC) membranes, was found to be around 81% and 97%, respectively. The rejection rates for Mg^{2+} and SO_4^{2-} were greater than that of Na^+ and Cl^-, which can be explained by a size exclusion mechanism. The mass transfer coefficient of $MgSO_4$ is greater than that of NaCl [53], making it difficult for Mg^{2+} and SO_4^{2-} to permeate through the membrane. Furthermore, the hydrated ionic radii of divalent ions, in solution, are larger than that of monovalent ions [54]. It is clear that the ZnO NPs modified PMAA-g-PA(TFC) membranes show better desalination performance when compared to PMAA-g-PA(TFC) membranes. The nano-modified membranes (0.1 wt. % of ZnO NPs) show a retention of 97% of total salinity, 99% of bivalent ions (Ca^{2+}, $SO_4^{2-}$and Mg^{2+}), and 98 % of monovalent ions (Cl^- and Na^+).

Table (2): Saline groundwater characterization before and after desalination process

Analytical parameter	Rejection sequence	TDS (mg/L)	Ca	Mg	Na	K	CO_3	HCO_3	SO_4	Cl
			(mg/L)							
Feed (PPm)	$Na^+ > Mg^{2+} > Ca^{2+} : Cl^- > SO_4^{2-} > HCO_3^-$	35264	2880	1847	14500	385	0.0	76.3	2508	30450
Product* (PPm)		6598	346	170	1812	69	0.0	22	189	4001
% Rejection*	$Mg^{2+} > Ca^{2} > Na^+ > K^+ : SO_4^{2-} > Cl^- > HCO_3^-$	81	88	91	87	82	0.0	71	92	87
Product (PPm)**		1133	49	21	335	15	0.0	10	22	685
% Rejection**	$Mg^{2+} > Ca^{2+} > Na^+ > K^+ : SO_4^{2-} > Cl^- > HCO_3^-$	97	98	99	97.7	96	0.0	87	99	98

Mg/L= Milligram/liter; *= PMAA-g-PA(TFC); **= ZnO NPs modified PMAA-g-PA(TFC) membrane.

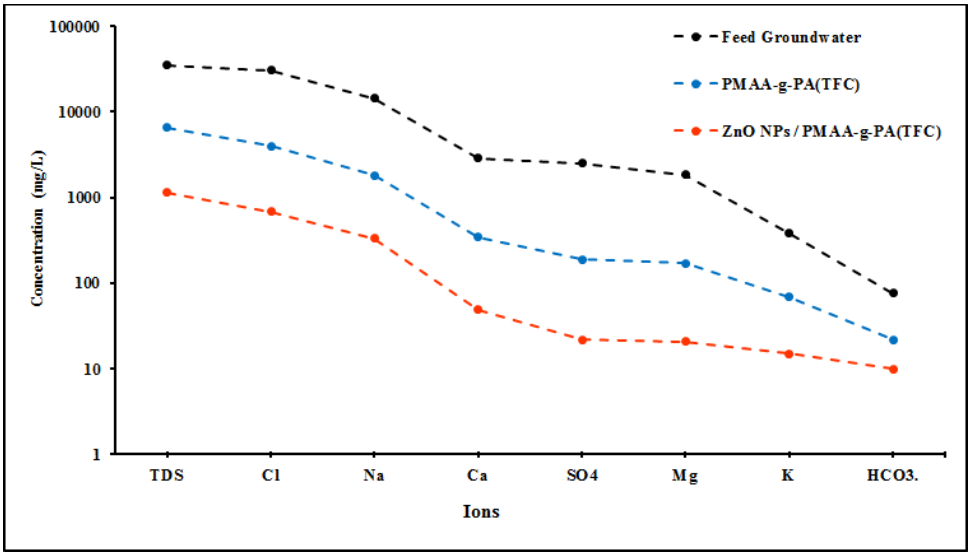

Fig. 10: Logarithmic diagram showing the membrane desalination performances for the PMAA-g-PA(TFC) and ZnO NPs modified PMAA-g-PA(TFC) membranes. Saline groundwater (35264 mg/L) sample has been used as feed water.

3.2.9. Stability of Zinc ions-containing membranes:

Determination of the release rate of zinc ions from ZnO NPs modified PMAA-g-PA(TFC) membranes would indicate the stability and efficiency of the modified membrane. To determine the release rate of zinc ions from the membrane surface, a batch experiment was carried out for ten days. The initial total amount of ZnO NPs incorporated in the membrane was estimated at 0.00778 µg/cm^2, which is equivalent to 0.00623 µg/cm^2 of Zn ion. Figure 11 shows the cumulative release of zinc ions during the first four days was 0.085µg/cm^2/day, which represent 85% of the total zinc ions released over the duration of the ten day experiment. The release rate achieves steady state after 6 days, where the amount of release has declined steadily with time to below 0.01 µg/cm^2 /day. The total amount of the Zn ions that has been leached out was estimated as 0.0.017 µg during the 10 days, representing 3.32 % the initial zinc ions incorporated on the graft modified membrane. The high release percent of Zn ions shown during the first four days is mainly due to the dissolution of unreacted ZnO NPs embedded on the membrane surface, which has been confirmed previously by SEM, Figure 5. The low total Zn ion release rate over the 10 day experiment indicates high stability and fixation of the ZnO NPs on the modified membrane surface.

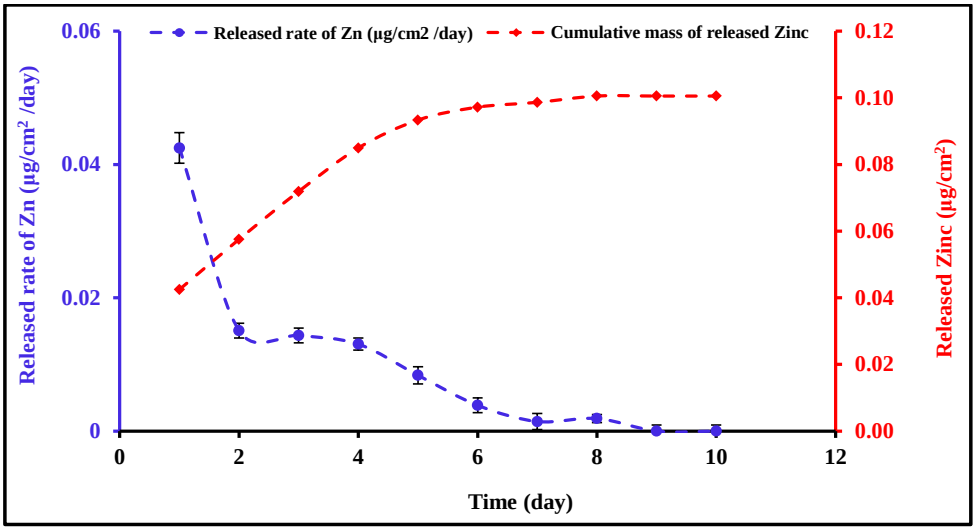

Fig. 11: Zinc ion release from the batch experiment, during the batch test, membrane samples were incorporated in 20 ml DI water under 120 rpm and the water was replaced every 24 h.

4. Antibacterial properties of membrane surfaces

The development of low-cost and effective technology is needed to address the problems associated with the harmful impacts of microorganisms on membrane surfaces. Biofouling is one of the largest challenges in membrane separation processes, where submerged membranes, in fresh or saline water, attract microorganisms including bacteria, algae and diatoms [55]. In this work, effective photocatalytic removal of *Escherichia coli* (*E. coli*) from aqueous solutions was reported using ZnO NPs under UV light irradiation. Zinc oxide (ZnO) is a nontoxic material with high photocatalytic activity. In visible light, zinc oxide absorbs onto the surface of the membrane, leading to in situ generation of hydrogen peroxide (H_2O_2) which acts as an antifouling agent [56].

The photocatalytic bactericidal ability of composite PA(TFC), PMAA-g-PA(TFC) and ZnO NPs modified PMAA-g-PA(TFC) membranes was tested by measuring *E. coli* (initial concentration = $670\times10^{+6}$ CFU/ml) survival under UV light exposure. Figure 12 shows the *E. coli* removal efficiency in water on different PA(TFC), PMAA-g-PA(TFC), and ZnO NP modified PMAA-g-PA(TFC) membrane surfaces under UV light. The antibacterial activity of the PMAA grafting layer was significantly improved by the addition of ZnO NPs. In comparison, the UV light alone exhibited slightly less antibacterial activity, where 66% of the *E. coli* cells survived after 90 minutes under UV illumination (initial concentration $5x10^4$ CFU/ml [57]. The survival count percentages of the *E. coli* cells was 12% on the neat PA(TFC) membrane, 6% on the PMAA-g-PA(TFC), and 0% on the ZnO NPs modified PMAA-g-PA(TFC) membrane, after 90 minutes of UV light exposure. These results were compared to the initial concentrations of the *E. coli* solution. *E. coli* survival was greatest on the PA(TFC) membranes, and lowest on the ZnO NPs modified PMAA-g-PA(TFC) membranes. The grafting of MAA monomers with carboxylic groups can enhance the negative surface charge of the PA(TFC) membrane which improves the antibacterial capabilities of the membrane surface, due to the negative surface charge of *E. coli* [58].

These results indicate, that the ZnO NPs modified PMAA-g-PA(TFC) membranes are able to eliminate *E. coli* more efficiently than pure (TFC) or PMAA-g-PA(TFC) membranes, due to the photocatalytic

bactericidal effect of the ZnO catalyst. Nearly complete removal of *E. coli* occurred within 90 minutes of UV light exposure on ZnO NPs modified PMAA-g-PA(TFC) membranes. The bactericidal effect of UV/ZnO through photocatalytic antibacterial agents is due to the presence of reactive oxygen species such as $O_2^{\bullet}$-, H_2O_2, and $HO^{\bullet}$ generated by ZnO, or the direct UV illumination of the cells. In the presence of ZnO NPs, photocatalytic reactions occur at the coating surface with oxygen and water. These compounds have antifouling properties that oxidize organs and destroy the outer-shell of bacteria cells. The photocatalytic activities of the ZnO NPs take place based on the following mechanism [59]:

$$ZnO + h\nu \longrightarrow ZnO\,(h^{+}_{VB} + e^{-}_{CB}) \qquad ZnO\,(h^{+}_{VB}) + H_2O \longrightarrow ZnO + OH^{\bullet} + H^{+}$$

$$OH^{\bullet} \xrightarrow{\text{Attack}} \textit{E coli}\ \text{(or) any organic materials}$$

The repulsion effect between the surfaces of the *E. coli* and the grafting membrane leads to a decrease in bacteria growth. Also, the PMAA grafting layer shows an excellent biocompatibility. These results are consistent with the findings that ZnO semiconductors have better efficiency in photochemical degradation, and offer economic and ecological benefits compared to conventional methods.

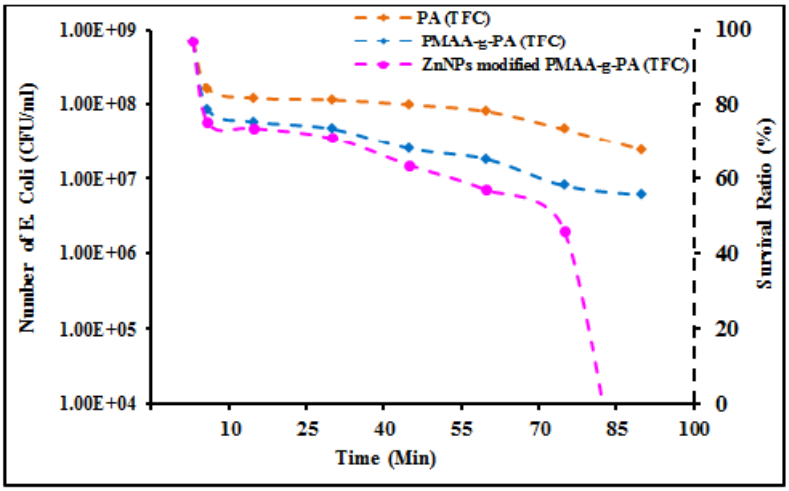

Fig. 12: Semi logarithmic curve and survival ratio of cell number of *E. coli* in PA(TFC), PMAA-g-PA(TFC) and ZnO NPs modified PMAA-g-PA(TFC) membranes.

5. Conclusions

Membranes were successfully synthesized by free radical graft polymerization of methacrylic acid (MAA) monomers onto a thin skin PA(TFC) active layer, over a microporous PS support, resulting in PMAA-g-PA(TFC) and ZnO NPs modified PMAA-g-PA(TFC) membranes. ZnO NPs were incorporated in aqueous grafting PMAA solution on the top layer of the PA(TFC) to enhance the dispersion of the ZnO NPs on the membrane surface. The incorporation of the ZnO NPs has greatly enhanced the mechanical properties of the modified membrane, where increases in the tensile strength (Mpa), the elongation break (%) and the estimated Young's modulus values were observed, and found to be greater than those of the other membranes. The performance of these membranes was evaluated with respect to permeability, water flux, salt rejection, and antibacterial activity using *E. coli* as a potential foulant. The ZnO NPs modified PMAA-g-PA(TFC) modified

membranes were more hydrophilic, with an improved water contact angle (~50 ± 3°) over the PMAA-g-PA(TFC) (63 ± 2.5°). The new membrane showed a retention of 97% of total salinity, 99% of bivalent ions (Ca^{2+}, $SO_4^{2-}$and Mg^{2+}), and 98% of monovalent ions (Cl^- and Na^+). The water flux of ZnO NPs modified PMAA-g-PA(TFC) represents an improvement of 71.4% and 83% over the pure PA(TFC) and PMAA-g-PA(TFC) membranes, respectively. The batch test indicates the stability and well fixation of the ZnO NPs on the modified membrane surfaces, where 3.23% of the initial ZnO NPs were released over a 10 day experiment. Finally, the ZnO NPs modified PMAA-g-PA(TFC) offer the additional advantage of possessing greater antibacterial activity when compared to PMAA-g-PA(TFC) and pure PA(TFC) membranes. These experiments demonstrate that the ZnO NPs modified PMAA-g-PA(TFC) membrane can significantly improve selectivity, permeability and bio-antifouling properties of the membranes for water desalination.

6. Acknowledgements

This work is dedicated to the memory of Dr. Magdi El-Sayed, who was a PhD supervisor for one of the authors (HI) during 2013 – 2015. His research and supervision during the course of the study is much appreciated. Acknowledgement goes to the Egyptian Scientific Technology Development Funding (STDF) for technical support and for funding of the project. The authors also thank the University of Waterloo for offering HI a Visiting Graduate Studentship.

7. References

[1] S. Zhao, W. Yan, M. Shi, Z. Wang, J. Wang and S. Wang (2015), Improving permeability and antifouling performance of polyethersulfon eultrafiltration membrane by incorporation of ZnO-DMF dispersion containing nano-ZnO and polyvinylpyrrolidone. Journal of Membrane Science 478:105–116.

[2] Z.E. Hughes, J.D. Gale (2010), A computational investigation of the properties of a reverse osmosis membrane, J. Mater. Chem. 20:7788–7799
.
[3] J. Shen, C. Yu, H. Ruan, C. Gao, B. Bruggen (2013), Preparation and characterization of thin-film nanocomposite membranes embedded with poly (methylmethacrylate) hydrophobic modified multiwalled carbon nanotubes by interfacial polymerization. Journal of Membrane Science 442:18–26.

[4] S. Kulprathipanja (2003), Mixed matrix membrane development, Ann. N.Y. Acad. Sci. 984: 361–369.

[5] N. Misdan, W.J. Lau, A.F. Ismail (2012), Seawater Reverse Osmosis (SWRO) desalination by thin-film composite membrane—Current development, challenges and future prospects Desalination 287: 228–237.

[6] H. Zou, Y, Jin, J. Yang, H. Dai, X. Yu, J. Xu (2010), Synthesis and characterization of thin film composite reverse osmosis membranes via novel interfacial polymerization approach, Separation and Purification Technology 72: 256–262.

[7] A. L. Ahmad, A. A. Abdulkarim, B. S. Ooi, S. Ismail (2013), Recent development in additives modifications of poly ether sulfone membrane for flux enhancement, Chem. Eng.J.223: 246–267.

[8] C. Zhao, J. Xue, F. Ran, S. Sun (2013), Modification of poly ether sulfone membranes – a review of methods, Prog. Mater. Sci.58: 76–150.

[9] L. Yu, Y. Zhang, B. Zhang, J. Liu, H. Zhang, C. Song (2013), Preparation and characterization of HPEI-GO/PES ultrafiltration membrane with antifouling and antibacterialproperties,J.Membr.Sci.447 :452–462.

[10] S. Belfer, Y. Purinson, R. Fainshtein, Y. Radchenko, O. Kedem (1998a), Surface modification of commercial composite polyamide reverse osmosis membranes, J. Membr. Sci. 139: 175–181.

[11] D. Y. Chu, J. K. Thomas (1984), Photophysical studies of a water-soluble copolymer of methacrylic acid and 1-pyreneacrylic acid, Macromolecules 17: 2142 – 2147.

[12] J. Zhang, N. A. Peppas (2000), Synthesis and Characterization of pH and Temperature-Sensitive Poly(methacrylic acid)/Poly(N-isopropylacrylamide) Interpenetrating Polymeric Networks. Macromolecules, 33: 102-107.

[13] S. Li, M. S. Toprak, Y. S. Jo, J. Dobson, D. K. Kim, M. Muhammed (2007), Bulk Synthesis of Transparent and Homogeneous Polymeric Hybrid Materials with ZnO Quantum Dots and PMMA. Adv. Mater. 19: 4347–4352. DOI: 10.1002/adma.200700736.

[14] J. Zheng, R. Ozisik, R.W. Siegel (2005), Disruption of self-assembly and altered mechanical behavior in polyurethane/zinc oxide nanocomposites Polymer 46:10873–10882.

[15] J. N. Shen, H.M. Ruan, L.G. Wu, C.J. Gao (2011), Preparation and characterization of PES–SiO2 organic–inorganic composite ultrafiltration membrane for raw water pretreatment, Chem. Eng. J. 168(3) 1272–1278.

[16] J. Shen, C. Yu, H. Ruan, C. Gao, B. Bruggen (2013), Preparation and characterization of thin-film nanocomposite membranes embedded with poly (methylmethacrylate) hydrophobic modified multiwalled carbon nanotubes by interfacial polymerization. Journal of Membrane Science 442:18–26.

[17] Jun Yin, Yu Yang , Zhiqiang Hu, Baolin Deng (2013), Attachment of silver nanoparticles (AgNPs) onto thin-film composite (TFC) membranes through covalent bonding to reduce membrane biofouling. Journal of Membrane Science 441:73–82.

[18] M. L. Lind, A.K. Ghosh, A. Jawor, X. F. Huang, W. Hou, Y. Yang, E. M. V. Hoek (2009), Influence of zeolite crystal size on zeolite–polyamide thin film nanocomposite membranes, Langmuir 25(17) 10139–10145.

[19] J. Garcia-Ivars, M. Iborra-Clar, M. Alcaina-Miranda, J. Mendoza-Roca, L. Pastor-Alcañiz (2014), Development of fouling-resistant polyethersulfone ultrafiltration membranes via surface UV photografting with polyethylene glycol/aluminum oxide nanoparticles. Separation and Purification Technology 135:88–99.

[20] Y. Zhang, P. Cui, T. Du, L. Shan, Y. Wang (2009), Development of a sulfated Y-doped non stoichiometric zirconia / polysulfone composite membrane for treatment of wastewater containing oil, Sep. Purif. Technol. 70: 153–159.

[21] J. Lee, H.-R. Chae, Y. J. Won, K. Lee, C.-H. Lee, H. H. Lee, I.-C. Kim, J.-m. Lee (2013), Graphene oxide nano platelets composite membrane with hydrophilic and antifouling properties for waste water treatment. J. Membr. Sci. 448: 223–230.

[22] J. Kim, B. V. Bruggen (2010), The use of nanoparticles in polymeric and ceramic membrane structures: review of manufacturing procedures and performance improvement for water treatment, Environ. Pollut. 158: 2335–2349.

[23] K. H. Tam, A. B.Djurisic, C.M. N.Chan, Y. Y. Xi, C. W. Tse, Y. H. Leung, W. K. Chan, F. C. C. Leung, D.W. T. Au (2008), Antibacterial Activity of ZnO Nanorods Prepared by a Hydrothermal Method, Thin Solid Films, 516: 6167–6174.

[24] M.G. Nair, M. Nirmala, K. Rekha, A. Anukaliani (2011), Structural, optical, photo catalytic and antibacterial activity of ZnO and Co doped ZnO nanoparticles. Mater Lett; 65: 1797–800.

[25] X. Lou, S. Hesheng, S. Yusheng (1991), Development of ZnO series ceramic semiconductor gas sensors. J. Sens. Trans. Technol. 3: 1–5.

[26] Z. L. Wang (2008), Splendid one-dimensional nanostructures of zinc oxide: A new nanomaterial family for nanotechnology. ACS Nano, 2: 1987–1992.

[27] D. X. Wang, F. Tong, P. Aerts (2011), Application of the combined ultrafiltration and reverse osmosis for refinery wastewater reuse in Sinopec Yanshan Plant, Desalin, Water Treat. 25: 133–142.

[28] H. C. Flemming (1997), Reverse osmosis membrane biofouling, Experimental Thermal and Fluid Science 14: 382–391.

[29] W. Hu, C. Shiyan, B. Zhou, H. Wang (2010), Facile synthesis of ZnO nanoparticles based on bacterial cellulose, Mater. Sci. Eng. B 170: 88–92.

[30] A. B. Djurišcić, X. Y. Chen, Y. H. Lung (2012), Recent progress in hydrothermal synthesis of zinc oxide nanomaterials. Recent Pat. Nanotechnol. 6:124–134.

[31] D. K. Bhat (2008), Facile synthesis of ZnO nanorods by microwave irradiation of zinc–hydrazine hydrate complex. Nanoscale Res Lett 3:31.

[32] K. Chitra, G. Annadurai (2013), Antimicrobial activity of wet chemically engineered spherical shaped ZnO nanoparticles on food borne pathogen, International Food Research Journal 20(1): 59-64.

[33] A. Arora, S. Devi, V. S. Jaswal, J. Singh, M. Kinger and V. D. Gupta (2014), Synthesis and Characterization of ZnO Nanoparticles, Original Journal of Chemistry, ISSN: 0970-020 X CODEN: OJCHEG 2014, Vol. 30 (4): 1671-1679.

[34] Sadtler (1980), The Infrared Spectra Atlas of Monomers and P-3-N. Kwon and polymers: Sadtler Research Laboratories.

[35] S. Balta, A. Sotto, P. Luis, L. Benea, B. Van der Bruggen, J. Kim (2012), A new outlook on membrane enhancement with nanoparticles: The alternative of ZnO, J. Membr. Sci., 389: 155–161.

[36] J. Shen, C. Yu, H. Ruan, C. Gao, B. Bruggen (2013), Preparation and characterization of thin-film nanocomposite membranes embedded with poly (methylmethacrylate) hydrophobic modified multiwalled carbon nanotubes by interfacial polymerization. Journal of Membrane Science 442:18–26.

[37] Q. Cheng, Y. Zheng, S. Yua, H. Zhu, X. Penga, J. Liua, J. Liu, M. Liub, C. Gao (2013), Surface modification of a commercial thin-film composite polyamide reverse osmosis membrane through graft polymerization of N-isopropylacrylamide followed by acrylic acid. Journal of Membrane Science 1-46. 447: 236–245.

[38] M. M. Said, A. M. El-Aassar, Y. H. Kotp, H. A. Shawky and M.S.A. Abdel Mottaleb (2013) Performance assessment of prepared polyamide thin film composite membrane for desalination of saline groundwater at Mersa Alam-Ras Banas, Red Sea Coast, Egypt, Desalination and Water Treatment 1, DOI: 10.1080/19443994.2013.795208.

[39] H. S. Lee, S.J. Im, J.H. Kim, H.J. Kim, J.P. Kim, B.R. Min (2008), Polyamide thin-film nanofiltration membranes containing TiO2 nanoparticles, Desalination 219: 48–56.

[40] H. A. Shawky, S.-R. Chae, S. Lin, M.R. Wiesner (2011), Synthesis and characterization of a carbon nanotube/polymer nanocomposite membrane for water treatment. Desalination 272: 46–50.

[41] H. A. Shawky (2009) Performance of aromatic polyamide RO membranes synthesized by interfacial polycondensation process in a water-tetrahydrofuran system, J. Membr. Sci. 339: 209–214.

[42] S. Belfer, Y. Purinson, O. Kedem (1998b), Surface modification of commercial polyamide reverse osmosis membranes by radical grafting: an ATR-FTIR study, Acta Polym. 49: 574-582.

[43] J. Dechant, R. Danz, W. Kimmer, R. Schmolke (1972), Ultrarotspektroskopische Untersuchungen an Polymeren, Akademie-Verlag, Berlin, p. 269.

[44] M. Z. Rong, M. Q. Zhang, H. B. Wang, H. M. Zeng (2002), Surface modification of magnetic metal nanoparticals through irradiation graft polymerization. Appl. Surf. Sci. 200:76-93.

[45] E. Tang, G. Cheng, X. Maa, X. Pang, Q. Zhao (2006), Surface modification of zinc oxide nanoparticle by PMAA and its dispersion in aqueous system, Applied Surface Science, 252: 5227–523.

[46] R. Augustine, H. N. Malik, D. K. Singhal, A. Mukherjee, D. Malakar, N. Kalarikkal, S. Thomas (2014), Electrospun poly caprolactone/ZnO nanocomposite membranes as biomaterials with antibacterial and cell adhesion properties. J. Polym. Res., 21:347. DOI 10.1007/s10965-013-0347-6.

[47] M. Moniruzzaman, J. Chattopadhyay, W. E. Billups, K. I. Winey (2007), Tuning the Mechanical Properties of SWNT/Nylon 6,10 Composites with Flexible Spacers at the Interface, Nano Lett., 7(5): 1178-1185.

[48] H. Wu, B. Tang, P. Wu (2010), Novel ultrafiltration membranes prepared from a multi-walled carbon nanotubes/polymer composite. Journal of Membrane Science, 362 (1-2), 374–383.

[49] C. P. Leo, W.P. C. Lee, A. L. Ahmed, A.W. Mohammad (2012), Polysulfone membranes blended with ZnO nanoparticals for reducing fouling by oleic acid, Separation and purification technology, 89: 51-56.

[50] E. Tang, G. Cheng, X. Ma (2006) Preparation of nano-ZnO/PMMA composite particles via grafting of the copolymer onto the surface of zinc oxide nanoparticles. Powder Technology 161: 209 – 214.

[51] M. Mulder (1996), Basic Principles of Membrane Technology, 2nd ed., Kluwer Academic Publishers, Dordrecht.

[52] L. Shen, X. Bian, X. Lu, L. Shi, Z. Liu, L. Chen, Z. Hou, K. Fan (2012), Preparation and characterization of ZnO/poly ethersulfone (PES) hybrid membranes, Desalination 293, 21–29.

[53] J. Alam, L. A. Dass, M. Alhoshan (2013), Mixed- matrix membranes for desalination of water. Society of plastics Engineers, Plastics research online.

[54] M. Khayet, J. I. Mengual (2004), Effect of salt type on mass transfer in reverse osmosis thin film composite membranes, Desalination168: 383–390.

[55] Q. Zhu, J. Chen, Q. Zhu, Xing Fu Zhou (2010), Monodispersed hollow microsphere of ZnO mesoporous nanopieces: preparation, growth mechanism and photocatalytic performance, Materials Research Bulletin, 45(12): 2024–2030.

[56] Q. Li, S. Mahendra, D.Y. Lyon, L. Brunet, M.V. Liga, D. Li (2008), Antimicrobial Nanomaterials for Water Disinfection and Microbial Control: Potential Applications and Implications. Water Res., 42: 4591–4602.

[57] S. H. Kim, S. Kwak, B. Sohn, T. H. Park (2003), Design of TiO_2 nanoparticle self-assembled aromatic polyamide thin-film-composite (TFC) membrane as an approach to solve biofouling problem. Journal of Membrane Science 211: 157–165.

[58] A. Rezaee, A. K. J-Jafari, A. R. Khataee, A. Niliahmadabadi (2011), *Escherichia Coli* Removal from Water Using Electrophotocatalytic Method. Journal of Applied Sciences & Environmental Management, 15 (3) 439.

[59] A. Mostafaei, F. Nasirpouri (2013), Preparation and characterization of a novel conducting nanocomposite blended with epoxy coating for antifouling and antibacterial applications. J. Coat. Technol. Res., 10 (5) 679–694, DOI 10.1007/s11998-013-9487-1.